Inorganic Chemistry

Article

pubs.acs.org/IC

Multichannel-Emissive V-Shaped Boryl-BODIPY Dyads: Synthesis, Structure, and Remarkably Diverse Response toward Fluoride

Chinna Ayya Swamy P, Sanjoy Mukherjee, and Pakkirisamy Thilagar*

Department of Inorganic and Physical Chemistry, Indian Institute of Science, Bangalore 560012, India

Supporting Information

ABSTRACT: Three new V-shaped boryl-BODIPY dyads (**1**–**3**) were synthesized and structurally characterized. Compounds **1**–**3** are structurally close molecular siblings differing only in the number of methyl substituents on the BODIPY moiety that were found to play a major role in determining their photophysical behavior. The dyads show rare forms of multiple-channel emission characteristics arising from different extents of electronic energy transfer (EET) processes between the two covalently linked fluorescent chromophores (borane and BODIPY units). Insights into the origin and nature of their emission behavior were gained from comparison with closely related model molecular systems and related photophysical investigations. Because of the presence of the Lewis acidic triarylborane moiety, the dyads function as highly selective and sensitive fluoride sensors with vastly different response behaviors. When fluoride binds to the tricoordinate borane center, dyad **1** shows gradual quenching of its BODIPY-dominated emission due to the ceasing of the (borane to BODIPY) EET process. Dyad **2** shows a ratiometric fluorescence response for fluoride ions. Dyad **3** forms fluoride-induced nanoaggregates that result in fast and effective quenching of its fluorescence intensity just for ∼0.3 ppm of analyte (i.e., 0.1 equiv ≡ 0.26 ppm of fluoride). The small structural alterations in these three structurally close dyads (**1**–**3**) result in exceptionally versatile and unique photophysical behaviors and remarkably diverse responses toward a single analyte, i.e., fluoride ion.

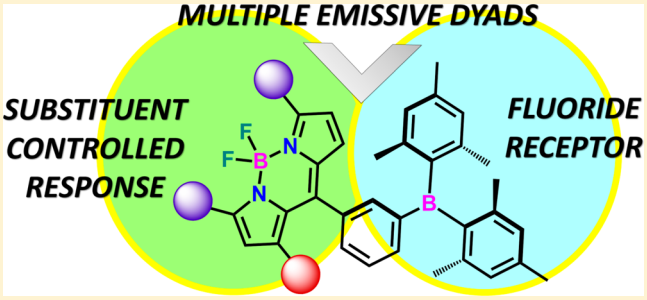

INTRODUCTION

The versatile photochemistry of boron-containing molecular materials has attracted considerable attention in the past few years.[1,2] Triarylboranes, because of their inherent electron deficiency, unique photophysical characteristics, and synthetic tunability, have found potential applications in the field of optoelectronic devices.[1] In 2001, Yamaguchi et al. demonstrated that boron-containing π-electron systems (Ar_3B), because of their inherent Lewis acidity and optimal steric bulk, can selectively detect the presence of small anions such as fluoride via Lewis acid base adduct (Ar_3BF^-) formation.[3] Later, Gabbai and co-workers demonstrated that detection of fluoride in water can also be achieved by triarylborane-containing water-soluble Lewis acids.[4] Triarylborane-based sensing platforms have been studied by several research groups.[1a,b,4,5]

Tetracoordinate boron-containing dyes have also been developed and found applications in modern materials chemistry.[6] In particular, the chemistry of BODIPY (borondipyrromethene) dyes have been extensively investigated and commercialized in bioimaging applications.[7] BODIPYs have also found potential applications as functional units in light-harvesting systems,[8] molecular sensors,[9] and semiconducting optoelectronic materials.[10]

Recently, a number of examples in which these two types of boron-containing functionalities have been incorporated into a single molecular backbone have been reported, i.e., borane–BODIPY conjugates. Although the photochemistries of boranes and BODIPYs started their journeys independently almost four decades ago, the first documentation of a borane–BODIPY dyad appeared only in 2008.[11] Following this report, a few more borane–BODIPY conjugates were reported by other groups, demonstrating that these materials can perform as efficient solid-state emitters or highly selective fluoride sensors.[12] Recently, we have demonstrated that covalently linked borane–BODIPY conjugates can exhibit multichannel emission bands arising from individual building units as a result of partial energy transfer from triarylborane (TAB) to the BODIPY unit, which is highly dependent on the conformational state of the molecular system.[13] These borane–BODIPY conjugates act as highly selective and sensitive fluoride sensors because of the inherent Lewis acidity of the TAB moiety, and the multichannel emission channels provide an elegant opportunity to measure the ratiometric response.

Herein, we present a series of borane–BODIPY dyads (**1**–**3**) in which the two functionalities are substituted at positions 1 and 3 of a phenyl spacer. The "V" shape structure of the molecules brings the two fluorescent chromophores into remarkable proximity. The relative orientations of the $BMes_2$ and BODIPY units also diminish the extent of conjugation,

Received: September 30, 2013
Published: May 6, 2014

   dx.doi.org/10.1021/ic402470a | *Inorg. Chem.* 2014, 53, 4813–4823

Scheme 1. Synthesis of 1−3

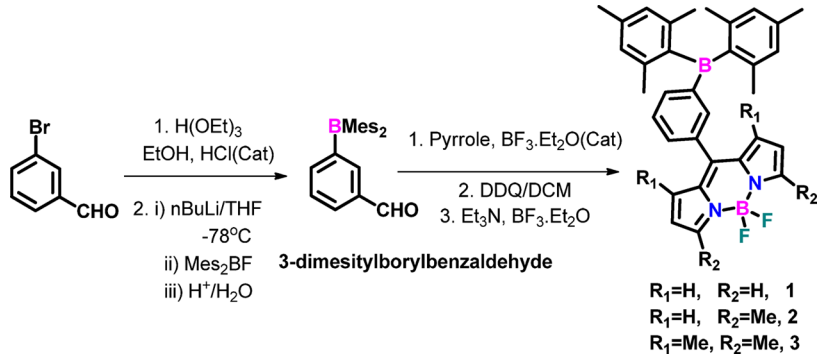

facilitating electronic energy transfer (EET) to become the dominant factor in controlling their emission characteristics. The EET processes in these dyads were found be highly affected by the methyl substituents on the BODIPY core. Additionally, the dyads were found to be highly selective and sensitive fluoride sensors with vastly different types of response behavior.

RESULTS AND DISCUSSION

Synthesis and Characterizations. Dyads **1**−**3** were prepared using conventional synthetic procedures[7] for BODIPYs (Scheme 1) starting from 3-dimesitylborylbenzaldehyde. Compounds **1**−**3** were characterized by NMR (^{1}H, ^{13}C, ^{19}F, and ^{11}B) and HRMS. Further, molecular structures of all the dyads were also confirmed by single-crystal X-ray diffraction studies (Figure 1).

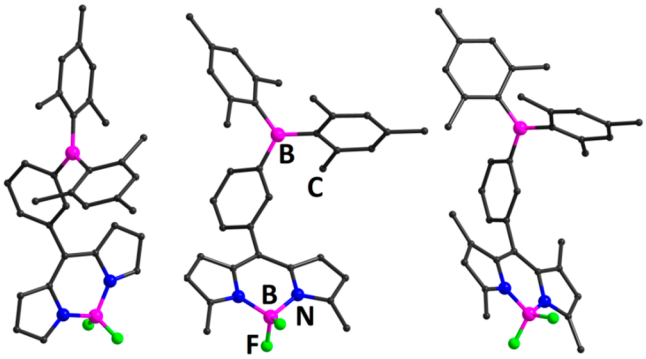

Figure 1. Molecular structures of **1** (left), **2** (middle), and **3** (right) as determined by single-crystal X-ray diffraction.

The ^{11}B NMR signals of the dyads show two distinctly separate signals for four-coordinate boron and three-coordinate boron centers in the regions of ∼1−2 and ∼65−70 ppm, respectively (see the Supporting Information). The ^{19}F NMR spectra of the dyads reveal a valuable qualitative insight into the molecular environment of the corresponding dyads. The shapes of ^{19}F resonances of **1**−**3** are sensitive to the number of methyl substituents on the pyrrole moiety of the indacene unit. Dyad **1** shows a typical quartet at −145.0 ppm; compound **2** gives rise to a broad multiplet at −147.5 ppm, and compound **3** shows a multiplet (overlap of two distinctly different quartet signals) at −146.3 ppm. This particular pattern of ^{19}F resonances may be due to the inequivalence of the two fluorines in the BF_2 unit of compounds **2** and **3**. Rotation of the meso-aryl-B(Mes_2) groups must be restricted by the neighboring 1,7-hydrogens (**2**) or 1,7-methyl units (**3**) to cause the two fluorines to reside in different chemical environments. Similar restricted rotation behavior of BODIPYs has been reported in the literature.[14] The minor resonances in the ^{19}F NMR spectra of **3** may be arising from coupling of the fluorine atoms to the ^{10}B nucleus.

Crystal Structures of 1−3. Single-crystal X-ray diffraction yielded structures of the dyads that were found to provide valuable information about the molecular environments. The crystallographic data and refinement details are listed in Table 1. Dyads **1** and **2** were found to be crystallized in the triclinic P$\bar{1}$ space group, whereas compound **3** crystallized in the monoclinic *Pc* space group. The asymmetric units of **1** and **2** contain only one crystallographically unique molecule, whereas for **3**, there are two crystallographically independent molecules in the asymmetric unit. The interplanar angle between the BODIPY core and the phenyl ring increases from **1** to **3** (39.2° for **1**, 50.9° for **2**, and 73.3° and 86.2° for two different asymmetric units in **3**). Interestingly, the interplanar angle

Table 1. Crystallographic Data of 1−3

	1	2	3
empirical formula	$C_{33}H_{32}B_2F_2N_2$	$C_{35}H_{36}B_2F_2N_2$	$C_{37}H_{40}B_2N_2F_2$
Fw	508.49	544.28	572.33
T (K)	293(2)	293(2)	293(2)
crystal system	triclinic	triclinic	monoclinic
space group	P$\bar{1}$	P$\bar{1}$	*Pc*
a (Å)	10.859(5)	8.3027(11)	20.3206(14)
b (Å)	11.642(5)	11.3660(16)	11.9014(9)
c (Å)	13.179(5)	16.543(2)	13.1195(9)
α (deg)	67.298(5)	80.372(9)	90
β (deg)	67.374(5)	80.281(9)	91.995(4)
γ (deg)	89.883(5)	70.038(9)	90
V (Å^3)	1397.6(10)	1436.1(3)	3170.9(4)
Z	2	2	4
ρ_{calcd} (g cm^{-3})	1.208	1.259	1.199
μ(Mo Kα) (mm^{-1})	0.079	0.078	0.076
λ (Å)	0.710 73	0.710 73	0.710 73
F (000)	505	506	1216
no. of reflections collected	22595	26652	46825
no. of unique reflections	4879	8112	11042
goodness of fit (F^2)	0.924	0.807	1.025
R_1 [$I > 2\sigma(I)$]^a	0.0769	0.0833	0.0763
wR_2 [$I > 2\sigma(I)$]^b	0.1419	0.2051	0.1956

$^a R_1 = \sum||F_0| - |F_c||/\sum|F_0|$. $^b wR_2 = \{\sum[w(F_0^2 - F_c^2)^2]/\sum[w(F_0^2)^2]\}^{1/2}$.

dx.doi.org/10.1021/ic402470a | Inorg. Chem. 2014, 53, 4813−4823

between the Ar_3B unit and BODIPY core is smallest in **2** (44.2°) and larger in **1** and **3** (88.7° for **1** and 88.3° and 69.7° for two different asymmetric units in **3**).

In the solid state, dyads **1** and **2** show oppositely directed and alternately arranged $\pi-\pi$ interactions between the neighboring BODIPY units (Figures 2 and 3). The $\pi-\pi$ distance between

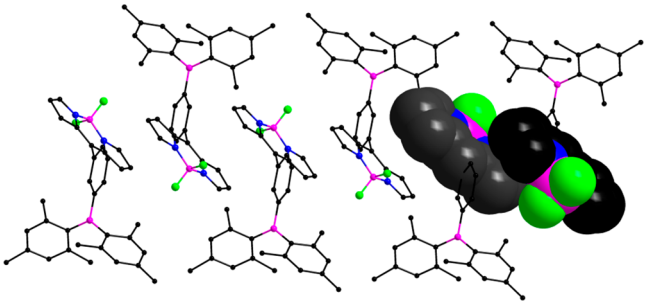

Figure 2. Solid-state structure of **1** (at the right, two BODIPY units are shown in space-fill representation to demonstrate the close $\pi-\pi$ interactions).

the adjacent BODIPY units in **1** is ~3.44 Å. In compound **2**, because of the incorporation of two additional methyl substituents at postions 3 and 5 of the BODIPY core, the intermolecular $\pi-\pi$ distance is relatively long (~3.72 Å) with respect to that in dyad **1**. Such $\pi-\pi$ interactions between the adjacent BODIPY units could not be observed in **3**, which can be attributed to the high degree of steric crowding around the BODIPY core (additional methyl substituents at positions 1, 3, 5, and 7 of the BODIPY core). Because of the suitable dihedral arrangement of the spacer phenyl moiety, weak intermolecular C−H···F interactions progress throughout the solid-state structures of **2** and **3** (Figure 3), which is not observed in **1**.

Computational Studies. To improve our understanding of the electronic behavior of dyads **1**−**3**, density functional theory (DFT) computational studies were performed at the B3LYP level considering the 6-311G(d) basis set for all atoms. The ground-state optimized structure of **1**−**3** closely resemble their solid-state crystal structures. The localized FMOs (frontier molecular orbitals) of the dyads indicate the absence of any significant electronic conjugation between the triarylborane and BODIPY moieties. Interestingly, the HOMO−LUMO band gap for **2** (2.96 eV) was found to be lower than those of **1** (3.08 eV) and **3** (2.99 eV). Although DFT-produced band gaps do not directly corroborate the experimentally observed (UV−vis) band gap values, the same trend of band gap increment (**2** < **3** < **1**) followed in experiments should be noted. From Figure 4,

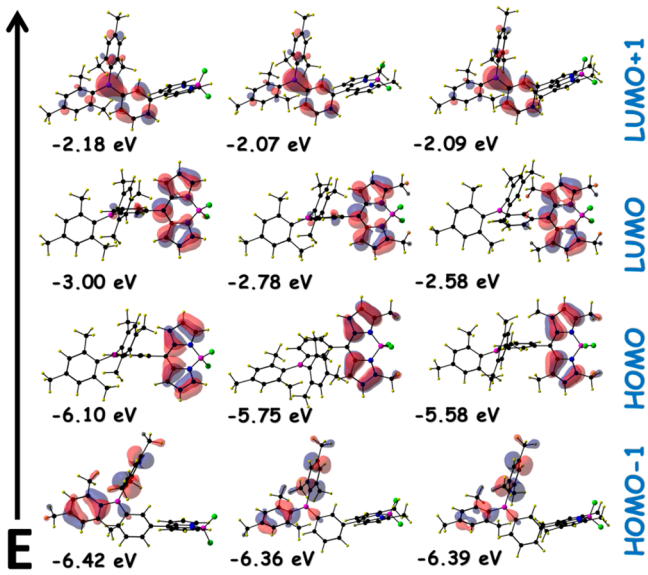

Figure 4. Selected MOs of **1** (left), **2** (middle), and **3** (right) as obtained from the DFT B3LYP/6-311G(d) level of computation (isovalue of 0.04).

it is evident that the σ^*(methyl)−π(BODIPY) [or σ^*-(methyl)−π^*(BODIPY)] interactions at the FMOs of **1**−**3** increase the energy levels of the corresponding orbitals. For **2**, the higher increment of the HOMO energy level results in its lowest HOMO−LUMO gap, whereas for **3**, the destabilization of the LUMO is also considerably strong because of the orthogonal arrangement of the phenyl spacer decreasing the level of effective conjugation, resulting in a HOMO−LUMO gap that is higher than that of **2** but lower than that of **1**. Excited-state optimizations for the dyads could not be achieved from the ground-state optimized structures because of the failure of convergence. However, ground-state and excited-state geometry optimizations of the computational models [**M1**−**M3** (Figure 5)] also provided useful insights into the role of the methyl substituents around the BODIPY core in controlling their photophysical behavior. As shown in Figure 5, model compound **M1** shows significant structural changes and puckering in its optimized first excited-state structure with respect to the ground-state structure, whereas for **M2** and **M3**,

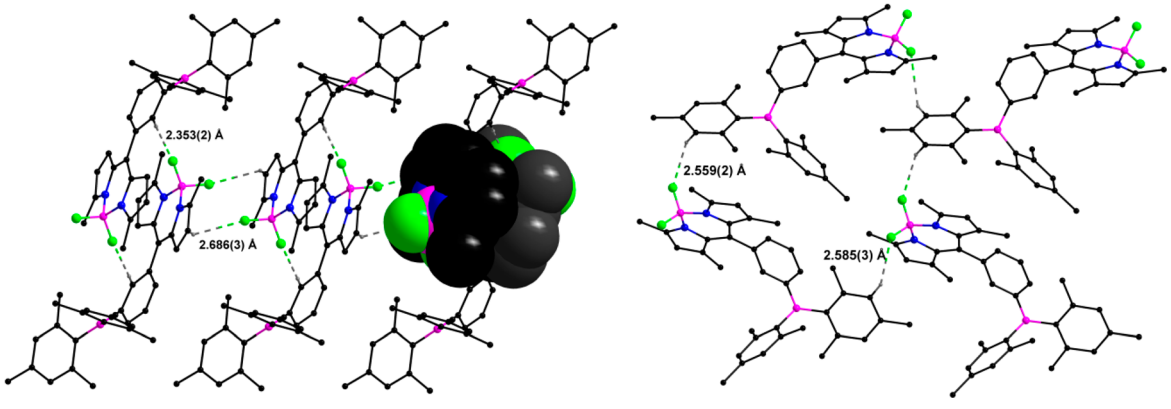

Figure 3. Solid-state weak C−H···F interactions in **2** (left) and **3** (right).

dx.doi.org/10.1021/ic402470a | Inorg. Chem. 2014, 53, 4813−4823

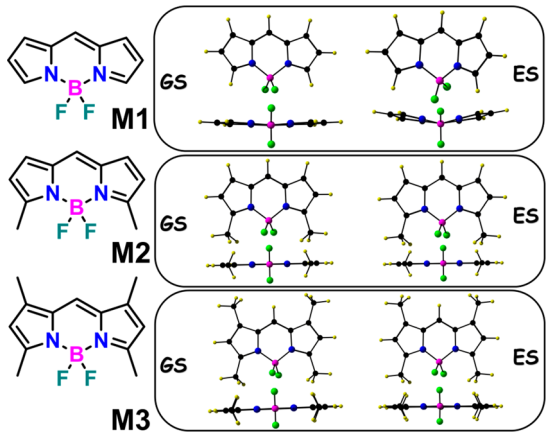

Figure 5. Computational models **M1**−**M3** (left) and their DFT B3LYP/6-311G(d) optimized ground-state (GS) and first excited-state optimized structures (ES).

such structural reorientations could not be followed. Therefore, the methyl substituents around the BODIPY moiety are expected to alter the excited-state, i.e., fluorescence, behaviors of the dyes to great extents. In particular, dyad **2** should experience the largest effects in this regard as in the case of **3**, the rigidity of the BODIPY core may be counter-effected by the neighboring vibrational and electronic couplings between the 2,7-methyl substituents and the meso-phenyl spacer. The experimentally observed optical behaviors of the dyads (**1**−**3**) corroborate these computational results.

Photophysical Properties. The absorption and fluorescence parameters of dyads **1**−**3** are listed in Table 2. The absorption spectra (Figure 6) of **1** and **3** are similar to absorption bands at ∼335 and ∼500 nm (with a shoulder at ∼475 nm). For **2**, the red-shifted bands observed at ∼350 and ∼510 nm are indicative of a lower HOMO−LUMO gap, which is also supported by DFT computational studies. The absorption regions (i.e., λ_{max}) of the dyads are almost not affected by solvent polarity (see the Supporting Information), which excludes any ground-state intramolecular charge transfer process (ICT) between the triarylborane and BODIPY entities. An absorption study of the dyads at different solution concentrations also excluded the presence of any significant ground-state intermolecular interactions in solution state (see the Supporting Information). Comparing the optical properties of **1**−**3** with those of model building blocks [**4**−**7** (Scheme 2)], we conclude that the absorption behavior of the dyads is the simple additive spectrum of the absorption profile of the individual chromophores (see the Supporting Information).

In emission studies (see Figure 2 and the Supporting Information), upon excitation at 350 nm, **1** and **3** were found to be dual emissive (λ_{em} at ∼405 and ∼515 nm) whereas **2** showed four distinct emission bands (λ_{em} at ∼405, ∼450, ∼495, and ∼525 nm) spanning a wide range of visible spectra. To understand the origin of this multiple-channel emission of the dyads, the emissions were compared to their model building units (**4**−**7**). The comparison showed that the ∼400 nm emissions of the dyads resemble the typical emission spectra of **7** whereas the ∼500−525 nm emission channels resemble the corresponding BODIPY building blocks (**4**−**6**). However, the additional features of the emission spectra of **2** could not be accounted for in this approach. As is evident from solid-state structures of dyad **2** (Figure 3), the BODIPY moieties tend to form closely packed $\pi-\pi$ interactions that may also occur in solution state, resulting in such broad emission features arising from molecular aggregates. However, to ascertain that the emission features of the dyads were arising from the molecular origin and not from any aggregated entities, emission for all the dyads was also recorded at different concentrations [0.01−1.00 mM (Figure 7)]. The consistency of the emission features and relative intensities of the individual emission bands at different concentrations led us to conclude that all the emission features of the dyads arose from individual molecular entities with different extents of EET processes present, not from any dye aggregates. The excitation spectra of the respective emission bands of **1**−**3** (shown in the Supporting Information) clearly demonstrated the active participation of the borane-dominated absorption bands (∼350 nm) in the fluorescence emission process of these dyads. The EET is relatively stronger in **3** than in **1** or **2**, which may be a result of the relative orthogonal arrangements of the TAB and BODIPY units (Table 2). The quantum yields of the dyads increase gradually on going from **1** (0.48) to **2** (0.55) to **3** (0.72) with increasing molecular rigidity, which can be corroborated by the previous discussions about the ^{19}F NMR signal patterns and DFT computational results. Also, the multiple-emission behavior of dyad **2** can also be corroborated by the DFT computational studies as well as the single-crystal solid-state structure in which the relatively less orthogonal dihedral arrangements of the $\mathbf{Ar_3B}$ units and the BODIPY core may be responsible for the partial transfer of energy from triarylborane to the BODIPY moiety.

Fluoride Binding Studies. Triarylboranes ($\mathbf{Ar_3B}$) are well-known fluoride receptors[3−5] and show photophysical responses upon binding of fluoride that result in formation *in situ* of the $\mathbf{Ar_3BF^-}$ entity. These photophysical responses are potentially useful in utilizing triarylborane-containing luminogens as fluoride-sensing platforms, and such sensing−recognition events can also provide key information regarding the neighboring electronic environment around the triarylborane core. Compounds **1**−**3** were found to be highly selective and sensitive to the presence of fluoride ions. In all cases, the saturation of their fluorescence responses is achieved upon addition of only 1.0 equiv of fluoride, resulting from the

Table 2. Photophysical Data of Dyads 1−3[a]

	absorption (nm) (ε)		emission (nm) (λ_{ex} = 350 nm)	quantum yield[b] (λ_{ex} = 350 nm)	EET efficiency (%)[c]
1	335 (4.6×10^4)	500 (9.2×10^4)	408, 519	0.48	∼69
2	340 (2.4×10^4)	515 (6.6×10^4)	405, 450, 491, 526	0.55	∼78
3	325 (2.5×10^4)	502 (1.0×10^5)	408, 515	0.72	∼84

[a]All given data are for 10 μM DCM solutions. [b]Quantum yields were calculated using a quinine sulfate (0.1 M H_2SO_4; λ_{ex} = 350 nm; Φ_F = 57.7%) solution as a reference and using the formula $\Phi = \Phi_F \times I/I_R \times A_R/A \times \eta^2/\eta_R^2$, where Φ is the quantum yield, I is the intensity of emission, A is the absorbance at λ_{ex}, and η is the refractive index of solvent. [c]EET efficiency = [(emission intensity of acceptor in dyad) − (emission intensity of donor in dyad)]/(emission intensity of free donor, i.e., model compound Mes_2BPh).

dx.doi.org/10.1021/ic402470a | *Inorg. Chem.* 2014, 53, 4813−4823

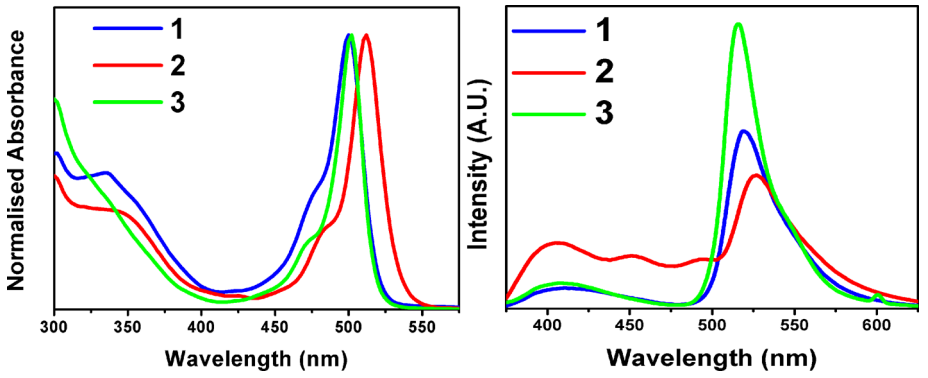

Figure 6. Normalized absorption spectra (left) and emission spectra (λ_{ex} = 350 nm) of **1**−**3** (right) at a concentration of 10 μM in DCM.

Scheme 2. Structures of Model Molecular Systems Used for Comparative Photophysical Investigations

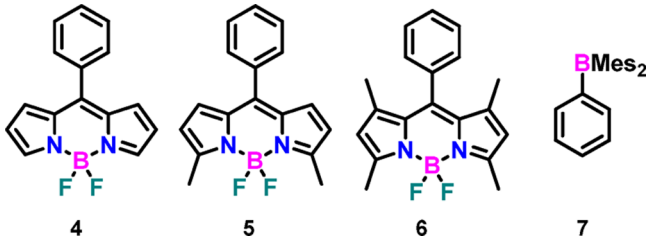

formation of a 1:1 complex. However, other anions, including CN^-, did not result in any such response.

1−**3** showed an almost similar kind of change in absorption spectra upon addition of TBAF [as, tetrabutylammonium fluoride (Figure 8)]. An average 5 nm blue shift of the BODIPY band accompanied by the decay of the boryl absorption band was observed for all the compounds. The complete saturation level for **1**−**3** was observed only after addition of ∼1.0 equiv of TBAF. The NMR studies (^{1}H, ^{11}B, and ^{19}F) before and after the addition of fluoride did not show any signs of chemical reactions or structural breakdown of the dyads (**1**−**3**) in the presence of even 50 equiv of fluoride (see the Supporting Information). Further, the intact shape and intensity of the BODIPY absorption bands confirmed the stability of the BODIPY core in the presence of fluoride. However, the emission responses of the dyads are remarkably different from one another.

The fluorescence titration spectra of **1** and **3** (10 μM in DCM; λ_{ex} = 350 nm) are shown in Figure 9. In both compounds, the boryl to BODIPY EET process was expected to change upon addition of fluoride as the boryl fluorophore would no longer be available. As shown in the results, in both the cases the intensity of only the BODIPY emission band was quenched significantly after addition of fluoride (Stern−Volmer quenching constant K_{sv} of 8.0 × 10^5 M^{-1}; UV−vis titration yielded a binding constant K_a of 1.4 × 10^5 M^{-1} for **1**). Compound **1** showed an 83% decrease in BODIPY fluorescence upon addition of only 1.0 equiv of fluoride. This certainly indicates that the fluorescence quenching is a result of the ceasing of the EET process from TAB to BODIPY. This behavior is similar in nature to that of our previously reported linear compact boryl−BODIPY dyads.[13]

Like compound **1**, compound **3** also showed quenching of the BODIPY fluorescence upon addition of TBAF, but its response appears to be significantly more sensitive (for **3**, K_{sv} = 2.6 × 10^6 M^{-1} and K_a = 2.2 × 10^5 M^{-1}). The addition of 0.1 equiv (i.e., 0.26 ppm) of fluoride results in a sudden blue-shift and weakening of absorption bands (Figure 10). When the sample was allowed to stand, the intensity of the absorption bands significantly recovers and the retrieval process stops at ∼15 min. Similarly, compound **3** loses ∼60% of its emission intensity after addition of only 0.1 equiv of fluoride (0.26 ppm). The emission intensity of the solution slowly recovers over a period of ∼15 min to nearly ∼91% of its initial value. If the quenching of fluorescence is a reflection of the electronic environment around individual molecular units, such rapid quenching of fluorescence is not to be expected. Also, the dynamic changes in UV−vis spectral patterns cannot be explained on the basis of the involvement of a single molecule. The dynamics of the fluoride binding event could be due to the formation of anion (fluoride)-induced molecular aggregation formation and segregation (over a period of time). To understand the possible aggregation process in detail, a series of DLS (dynamic light scattering) experiments were performed.

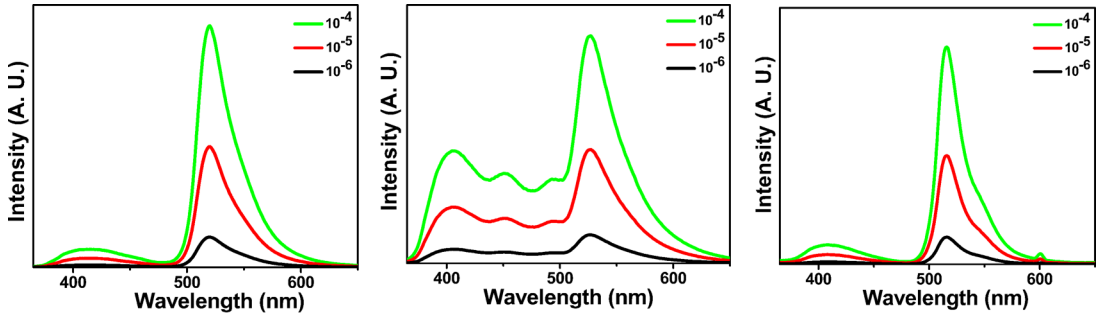

Figure 7. Emission (right) spectra of **1** (left), **2** (middle), and **3** (right) at different concentrations (DCM; λ_{ex} = 350 nm; numbers represent the molarity of the dyads in solution).

dx.doi.org/10.1021/ic402470a | Inorg. Chem. 2014, 53, 4813−4823

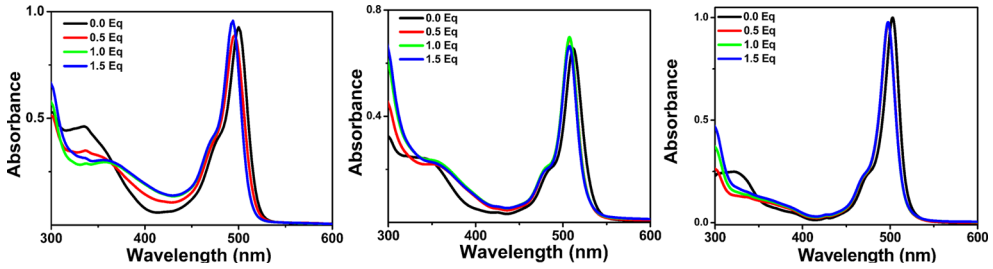

Figure 8. Spectral changes in the absorption spectra of **1** (left), **2** (middle), and **3** (right) in DCM (10 μM, DCM) upon addition of TBAF.

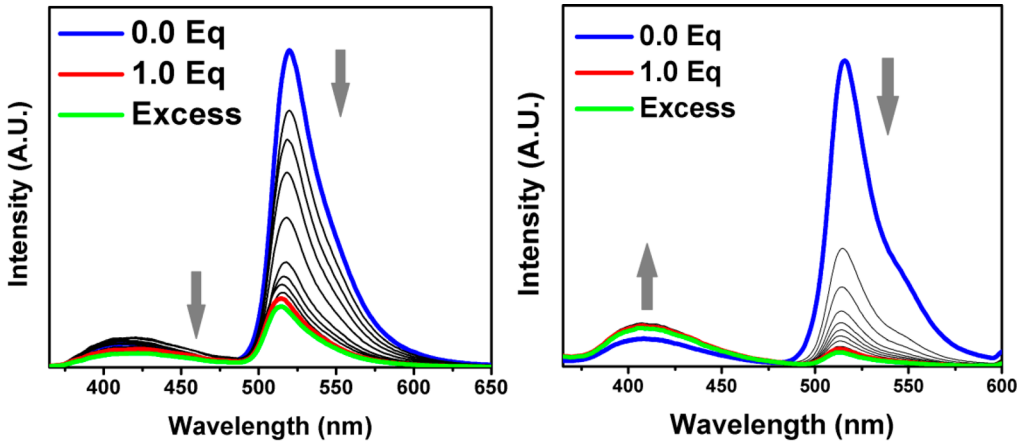

Figure 9. Spectral changes in the emission spectra of **1** (left) and **3** (right) in DCM (10 μM, DCM) (λ_{ex} = 350 nm) upon addition of TBAF.

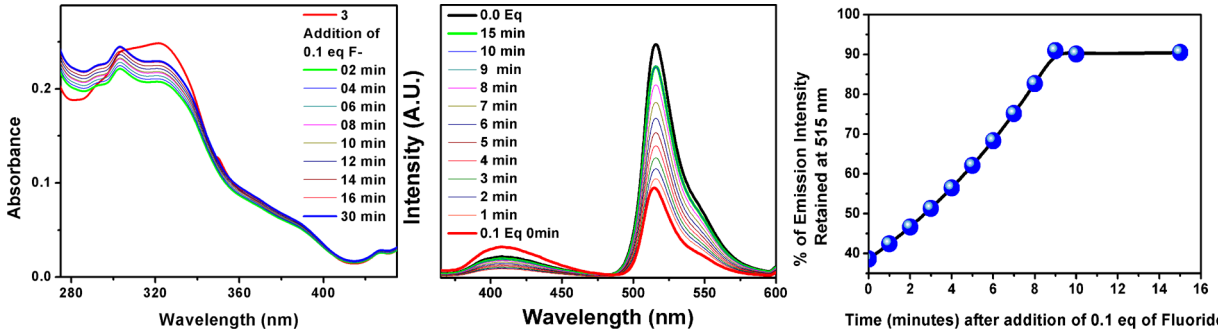

Figure 10. Partial UV–vis (left; only the higher-energy region is shown; for full spectra, see Figure S10 of the Supporting Information) and fluorescence titration spectra (10 μM, DCM; λ_{ex} = 350 nm) of **3** (middle) upon addition of 0.1 equiv of TBAF and its evolution with time (right).

In the absence of fluoride ion, compounds **1**–**3** do not form any aggregates at concentrations ranging from 1 mM to 1 μM (Figures S44, S46, and S48 of the Supporting Information). Also, compounds **1** and **2** do not form any aggregates upon addition of TBAF on short time scales or after standing for long periods of time (Figures S45 and S47 of the Supporting Information). Interestingly, compound **3** (10 μM solution) forms aggregates with an average diameter of ~325 nm in the presence of even small quantities of TBAF (0.1 equiv) (Figures S49–S55 of the Supporting Information). When the aggregates are allowed to stand, their average diameter gradually decreases (Figure 11 and Figures S48–S55 of the Supporting Information), a clear indication of the consecutive segregation process occurring on standing of the system (Figures S48–S55 of the Supporting Information). In corroboration with spectroscopic studies, the segregation process reaches completion within <15 min. Undoubtedly, the formation of the nonemissive aggregates upon addition of TBAF results in the fast fluoride-induced fluorescence quenching of **3**. Successively, the segregation process can easily explain the fluorescence recovery process observed over a period of ~15 min. To the best of our knowledge, although well-known in polymeric or supramolecular systems,[16] this type of cascade quenching behavior in molecular sensors is an unexplored area that needs further detailed studies and understanding. Anion-induced aggregation has been utilized in molecular probes, but such dynamic aggregation–segregation processes have not been explored in molecular sensors.[17] Such cascade quenching responses can be highly effective in detecting smaller amounts of target analytes.

As mentioned earlier, among the dyads **1**–**3**, the interplanar angle between the R_3B unit and the BODIPY moiety is smallest for **2**, which may be responsible for its unique emission characteristics. In the case of fluoride sensing also, **2** behaves anomalously. Upon addition of fluoride, dyads **1** and **3** showed a decrease in BODIPY fluorescence, resulting from the ceasing of EET from TAB to BODIPY. However, they did not show any significant recovery of the high-energy fluorescence band.

dx.doi.org/10.1021/ic402470a | *Inorg. Chem.* 2014, 53, 4813–4823

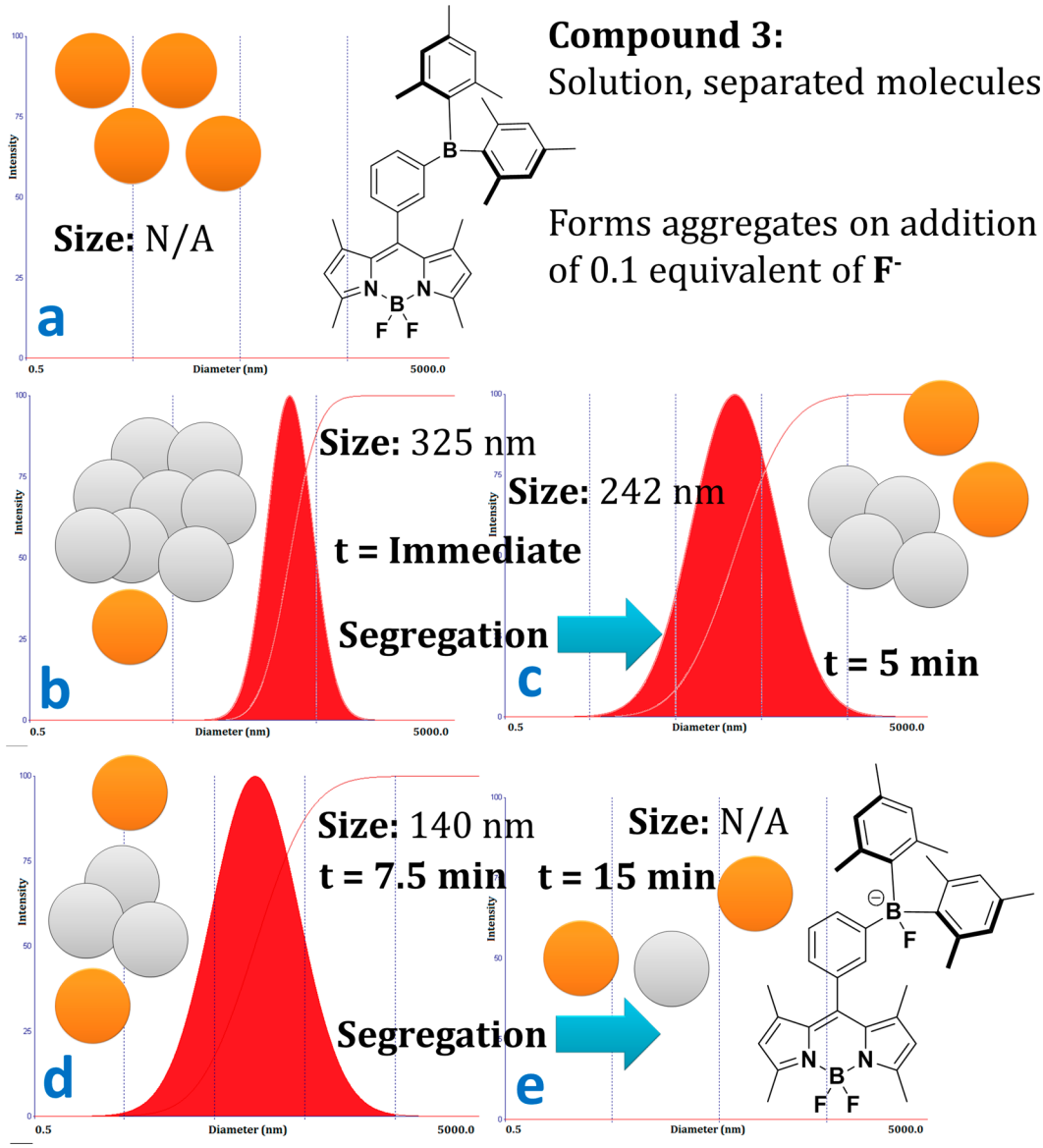

Figure 11. DLS measurement data and schematic (qualitative) representation of the fluoride-induced (0.1 equiv) aggregation process in compound **3** and the consecutive segregation process occurring over a short period of time. The DLS measurements were taken under the following conditions: (a) 10 μM solution of **3**, (b) immediately after the addition of 0.1 equiv of TBAF to the 10 μM solution of **3**, (c) 5 min after the addition of 0.1 equiv of TBAF to the 10 μM solution of **3**, (d) 7.5 min after the addition of 0.1 equiv of TBAF to the 10 μM solution of **3**, and (e) 15 min after the addition of 0.1 equiv of TBAF to the 10 μM solution of **3** (N/A, not applicable). The orange spheres represent compound **3**, whereas the gray spheres in panel e represent **3**·F^-.

For **2**, upon gradual addition of fluoride, we observed a steady decrease in BODIPY emission, which was accompanied by a steady increase in the intensity of the high-energy emission band at ~405 nm (for **2**, $K_{sv} = 3.1 \times 10^5\ M^{-1}$ and $K_a = 1.0 \times 10^5\ M^{-1}$). Thus, **2** behaved as a ratiometric fluorescent sensor of fluoride (Figure 12). In our view, this emission results from aromatic moieties around the fluoride-bound borane. Solvent-dependent emission studies of **2** (see the Supporting Information) showed no prominent indications of charge transfer characteristics as the emission bands are unaffected by solvent polarity. On the basis of this observation, it can be concluded that such behavior can arise only from termination of EET processes (TAB to BODIPY) upon binding of fluoride. The intensity ratio at 405 nm with respect to 525 nm (I_{405}/I_{525}) was found to increase gradually from 0.5 initially to 3.5 after addition of 1.0 equiv of fluoride, reaching a saturation level (Figure 12). This type of linear calibration curve can be exploited in determining the absolute concentration of analytes as ratiometric responses intrinsically rectify environmental changes in molecular fluorescence. Although such ratiometric behavior has been well explored in ICT- and FRET-based systems,[16] these types of general EET-based ratiometric sensors, to the best of our knowledge, have not been described in the literature. Interestingly, compound **2** shows a linear ratiometric response (Figure 12). The titration plot (Figure S18 of the Supporting Information) at concentrations of 1 μM also shows the same linear ratiometric response. Even in the presence of a large excess of other anions (as their tetrabutylammonium salts, e.g., Cl^-, Br^-, I^-, ClO_4^-, $H_2PO_4^-$, HSO_4^-, NO_3^-, PF_6^-, and CN^-), compounds **1**–**3** do not show any significant emission changes with respect to their free states in solution (Figure 13). Hence, dyads **1**–**3** can effectively

dx.doi.org/10.1021/ic402470a | Inorg. Chem. 2014, 53, 4813–4823

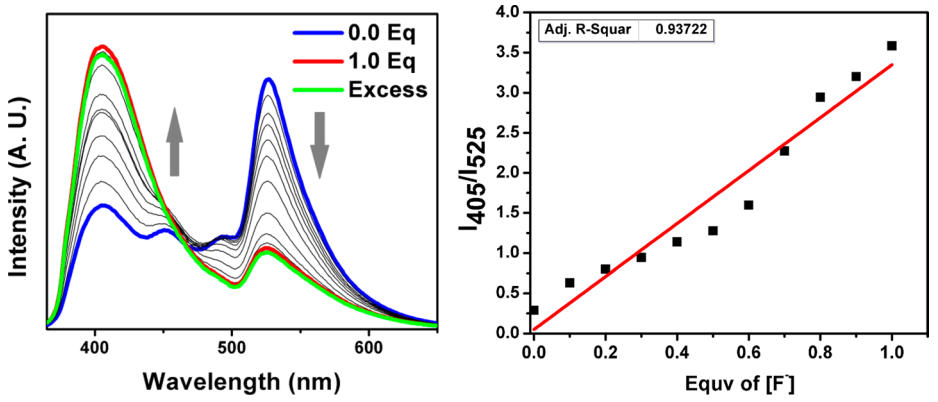

Figure 12. Fluorescence titration spectra of **2** (10 μM, DCM; λ_{ex} = 350 nm) upon addition of TBAF. The spectra were recorded immediately after addition. The right panel shows the change in the fluorescence intensity ratio (I_{405}/I_{525}) upon addition of fluoride.

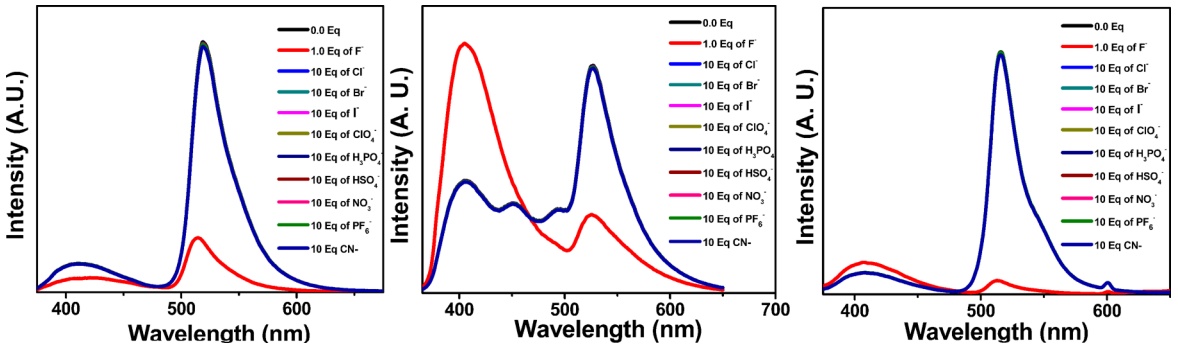

Figure 13. Fluorescence spectral changes of **1** (left), **2** (middle), and **3** (right) in the presence of different anions (10 μM, DCM; λ_{ex} = 350 nm; all anions were taken as the corresponding tetrabutylammonium salts).

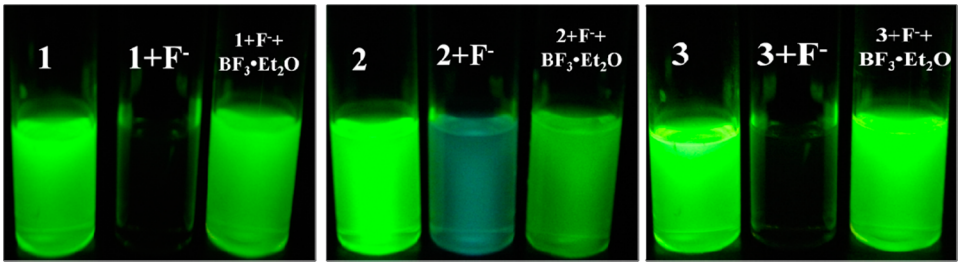

Figure 14. Digital photographs of the DCM solutions (10 μM) of dyads **1**–**3** (under UV light) after addition of 1.5 equiv of TBAF followed by subsequent addition of 1.5 equiv of $BF_3{\cdot}Et_2O$ (left, center, and right, respectively).

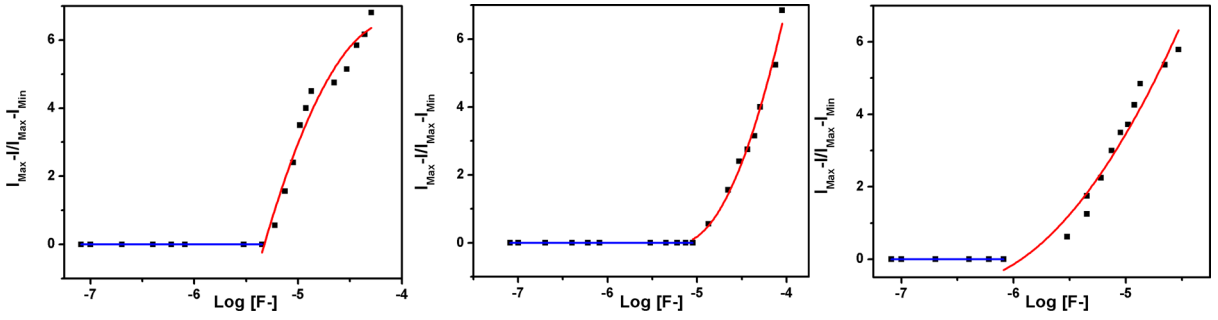

Figure 15. $(I_{max} - I)/(I_{max} - I_{min})$ vs log[F^-] plots for **1** (left), **2** (middle), and **3** (right). The intercept on the *X*-axis shows the lowest concentrations of [F^-] that can be detected by the respective sensors.

function as sensitive and selective fluorescent sensors for fluoride ions. The selectivity of the dyads (**1**–**3**) toward F^- with respect to other interfering species like CN^- is quite remarkable and can also be observed in other solvent systems, e.g., tetrahydrofuran (THF) (see the Supporting Information). The exclusive binding of fluoride is presumably facilitated by the small size of F^- and the relatively congested and compact structures of **1**–**3**. Such high selectivity is possibly caused by

dx.doi.org/10.1021/ic402470a | Inorg. Chem. 2014, 53, 4813–4823

the hardness of the Lewis acidic trivalent boron centers and reinforced by the neighboring electron deficient BODIPY core, which facilitates hard−hard (i.e., dyad−fluoride) interactions over hard−soft (i.e., dyad−cyanide) interactions. As shown in Figure 14, after following the fluorescence response of the dyads upon addition of fluoride ions, we were able to successfully regenerate the compounds via addition of an external reagent such as $BF_3{\cdot}Et_2O$. The more Lewis acidic nature of BF_3 assists in the removal of the borane-bound fluorides as tetrafluoroborate anions (BF_4^-) regenerating the luminescent dyads (**1**−**3**) *in situ*. Thus, by principle, the dyads can be recycled for subsequent usage. Further, the detection limits for the dyads (toward fluoride) were measured from the fluorescence quenching titration experiment. The intercept on the *X*-axis (here $\log[F^-]$) was obtained by linear fitting of $(I_{max} - I)/(I_{max} - I_{min})$ versus $\log[F^-]$, where I_{max}, I, and I_{min} are the initial fluorescence intensity, the intensity at a particular concentration, and the intensity at the saturation point, respectively. Detection limits were calculated by the formula ([F] × MWTBAF)/1000 (multiplied by 10^6 to change the units to parts per million), where MWTBAF is the molecular weight of TBAF (Figure 15). The detection limits for compounds **1** and **2** were found to be ∼1.2 and 2.3 ppm, respectively. Expectedly, the detection limit for compound **3** toward fluoride is ∼0.2 ppm, which is considerably improved compared to those of **1** and **2**. Clearly, the dyads act as highly sensitive receptors for fluoride ion under experimental conditions.

CONCLUSIONS

Three new V-shaped borane−BODIPY dyads were synthesized and structurally characterized using single-crystal X-ray diffraction. The dyads show multiple-channel emission that originates from individual molecular entities, not from any dye aggregates. Also, we have demonstrated how apparently mild structural fine-tuning in these conjugates can generate a family of versatile molecules with significantly different photophysical signatures and with vastly different fluoride responsive behavior with high selectivities and high sensitivities. The observation of a fluoride-induced aggregation process resulting in cascade quenching of fluorescence in compound **3** may open new opportunities for fast and sensitive detection strategies. The chemistry of broadly emissive organic molecules is yet to be well explored. Detailed phtotophysical as well as theoretical investigations of expanded related polychromophoric systems are currently underway in our research group.

EXPERIMENTAL SECTION

Materials and Methods. *n*-Butyllithium (1.6 M in hexane), 3-bromobenzaldehyde, and 2,3-dichloro-5,6-dicyano-1,4-benzoquinone (DDQ) were purchased from Aldrich, and pyrrole was purchased from SRL. All reactions were conducted under an atmosphere of purified nitrogen using standard Schlenck techniques. THF, pyrrole, and diethyl ether were distilled over sodium. Chlorinated solvents were distilled over CaH_2 and subsequently stored over 3 Å molecular sieves. The 400 MHz ^{1}H NMR, 376.5 MHz ^{19}F NMR, 100 MHz ^{13}C NMR, and 160.4 MHz ^{11}B NMR spectra were recorded on a Bruker Advance 400 MHz NMR spectrometer. All solution ^{1}H and ^{13}C spectra were referenced internally to the solvent signal. ^{11}B and ^{19}F NMR spectra were referenced externally to $BF_3{\cdot}Et_2O$ (δ = 0) in C_6D_6. Electronic absorption spectra were recorded on a PerkinElmer LAMBDA 750 UV/visible spectrophotometer. Solutions were prepared using a microbalance (±0.1 mg) and volumetric glassware and then charged in quartz cuvettes with sealing screw caps. Fluorescence emission studies were conducted on a Horiba JOBIN YVON Fluoromax-4 spectrometer. DLS measurements were conducted in a "Brookhaven Instruments Corp." platform. Single-crystal X-ray diffraction data were collected with a Bruker SMART APEX diffractometer equipped with a three-axis goniometer. The data were integrated using SAINT,[18] and an empirical absorption correction was applied with SADABS. The structures were determined by direct methods and refined by full matrix least squares on F^2 using SHELXTL.[18] All the non-hydrogen atoms were refined with anisotropic displacement parameters, while the hydrogen atoms were refined isotropically on the positions calculated using a riding model. The hybrid B3LYP functional has been used in all calculations as incorporated in Gaussian 09,[19] mixing the exact Hartree−Fock-type exchange with Becke's exchange functional and that proposed by Lee, Yang, and Parr for the correlation contribution. We used the 6-311G(d) basis set for all the atoms, which provides high-quality results on moderate time scales.

Synthesis of 3-Dimesitylborylbenzaldehyde. 3-Bromobenzaldehyde (9.5 g, 51.41 mmol) and triethyl orthoformate (113.24 mmol) were dissolved in ethanol, and then a catalytic amount of concentrated HCl was added to it. The resultant solution was refluxed for 4 h. After all the 3-bromobenzaldehyde had been consumed, the reaction mixture was brought to room temperature and extracted with a water/ethyl acetate mixture. The combined organic layer was washed with brine and dried over anhydrous Na_2SO_4. The volatiles removed under reduced pressure afforded 3-(diethoxymethyl)benzaldehyde as a colorless liquid. Yield: 14.28 g, 99%. ^{1}H NMR (400 MHz, $CDCl_3$): δ 7.65 [s, (*o*-Ph)], 7.35 [m, 2H (*o*,*m*-Ph)], 7.28 [d, J = 12 Hz, 1H (*p*-Ph)], 5.48 [s, 1H-(methine C-H)], 3.76−3.63 [m, 4H (-CH_2)], 1.28 [t, J = 6.8, 7.2 Hz, 6H (-CH_3)]. A solution of 3-(diethoxymethyl)-benzaldehyde (2.5 g, 9.64 mmol) in dry THF was degassed by being purged with N_2 for 30 min and then cooled to −78 °C (acetone and liquid N_2). *n*-BuLi [6.6 mL (1.6 M solution in hexane), 10.61 mmol] was added over 30 min. After 1 h, a solution of Mes_2BF (2.9 g, 10.08 mmol) in 15 mL of dry THF was added over 10 min. The reaction mixture was allowed to warm to room temperature, and stirring was continued for 12 h. After 12 h, 30 mL of 1 N HCl was added and stirring was continued for an additional 4 h and extracted with ether. The combined organic layers were washed with a brine solution and dried over anhydrous Na_2SO_4. Evaporation of the solvents under reduced pressure yielded the crude product. Recrystallization of the crude product in ethyl acetate gave pure **2** as a colorless solid. Yield: 2.35 g, 64%. ^{1}H NMR (399.99 MHz, $CDCl_3$): δ 9.89 (s, 1H), 8.01 [m, 2H (*o*-Ph)], 7.77 [d, J = 6 Hz, 2H (*m*-Ph)], 7.53 [d, J = 7.2 Hz, 1H (*m*-Ph)], 6.83 [s, 4H (Mes C-H)], 2.31, 1.98 [s, 18H (Mes-CH_3)]. ^{13}C NMR (100.00 MHz, $CDCl_3$): δ 193.4, 142.5, 141.2, 139.7, 138.6, 136.6, 132.2, 129.3, 128.9, 23.9, 21.7.

Synthesis of 1. Pyrrole (9 mL, 102.92 mmol) and 3-dimesitylborylbenzaldehyde (1.0 g, 2.82 mmol) were stirred in 100 mL of DCM at room temperature under a nitrogen atmosphere for 30 min, and then one drop of $BF_3{\cdot}Et_2O$ was added. After being stirred for 6 h, the reaction mixture was allowed to react with DDQ (116 mg, 0.51 mmol) in benzene (10 mL) for 6 h at room temperature. The resultant product was treated with triethylamine (0.7 mL, 4.6 mmol), and then $BF_3{\cdot}Et_2O$ (0.8 mL, 4.6 mmol) was added. The reaction mixture was stirred for an additional 5 h at room temperature, and the solvent was removed under vacuum to give the crude product, which was further purified by silica gel column chromatography (1:9 ethyl acetate/petroleum ether mixture) and yielded compound **1** as a red solid. Yield: 0.85 g, 74.34%. ^{1}H NMR (399.99 MHz, $CDCl_3$): δ 7.92 (s, β-pyrrolic 2H), 7.66 [d, J = 1.2 Hz, 1H (*o*-Ph)], 7.64 [d, J = 1.6 Hz, 1H (*m*-Ph)], 7.59 [s, 1H (*o*-Ph)], 7.52 [m, 1H (*p*-Ph)], 6.86 [s, 4H (Mes-C-H)], 6.81 [s, 2H (α-pyrrolic H)], 6.52 [d, J = 1.2 Hz, 2H (α'-pyrrolic H)], 2.29 [s, 6H (Mes-CH_3)], 2.02 [s, 18H (Mes-CH_3)]. ^{13}C NMR (100.00 MHz, $CDCl_3$): δ 148.0, 144.53 141.1, 139.8, 138.3, 137.6, 135.5, 134.0, 133.7, 132.1, 131.7, 130.9, 128.9, 128.5, 118.9, 23.9, 21.7. ^{11}B NMR (160 MHz, $CDCl_3$): δ 68.3 (bs), 1.23 (t, J = 36, 36 Hz). ^{19}F NMR (376 MHz, $CDCl_3$): δ −145.0 (q). HRMS (Q-TOF): calcd ($C_{33}H_{32}B_2F_2N_2Na$), 539.2617 Da; found, 539.2622 Da $[M + Na]^+$.

dx.doi.org/10.1021/ic402470a | *Inorg. Chem.* 2014, 53, 4813−4823

Synthesis of 2. 2-Methylpyrrole (0.21 g, 1.47 mmol) and 3-dimesitylborylbenzaldehyde (0.20 g, 0.56 mmol) were stirred at room temperature under a nitrogen atmosphere for 30 min, and then $BF_3{\cdot}Et_2O$ (13 μL, 0.19 mmol) was added. The resultant mixture was stirred for an additional 6 h at room temperature, and a solution of DDQ (0.28 g, 1.12 mmol) in benzene (10 mL) was added and stirring continued for an additional 6 h. The resultant solution was allowed to react with triethylamine (1.63 mL, 11.20 mmol) and $BF_3{\cdot}Et_2O$ (1.5 mL, 11.20 mmol). After the mixture had been stirred for 5 h at room temperature, the solvents were removed under vacuum to give the crude product, which was further purified by silica gel column chromatography (1:99 ethyl acetate/petroleum ether mixture) to give compound **2** as a greenish red solid. Yield: 30 mg, 20%. ^{1}H NMR (399.99 MHz, $CDCl_3$): δ 7.70 [d, J = 7.6 Hz, 1H (*o*-Ph)], 7.62 [m, 1H (*m*-Ph)], 7.54 [s, 1H (*o*-Ph)], 7.52 [d, J = 10.2 Hz, 1H (*p*-Ph)], 6.86 [s, 4H (Mes-C-H)], 6.64 [d, J = 4.0 Hz, 2H (α-pyrrolic H)], 6.24 [d, J = 4.0 Hz, 2H (α′-pyrrolic H)], 2.67 [s, 6H (β-CH_3)], 2.34, 2.22, 2.06 [s, 18H (Mes-CH_3)]. ^{13}C NMR (100.00 MHz, $CDCl_3$): δ 157.9, 143.2, 141.1, 139.6, 137.6, 135.1, 134.3, 133.6, 130.5, 129.0, 128.9, 128.2, 119.8, 23.8, 21.7, 15.3. ^{11}B NMR (160 MHz, $CDCl_3$): δ 67.1 (bs), 1.18 (t, J = 36, 36 Hz). ^{19}F NMR (376 MHz, $CDCl_3$): δ −147.5 (m). HRMS (Q-TOF): calcd ($C_{35}H_{36}B_2F_2N_2Na$), 567.2930 Da; found, 567.2934 Da $[M + Na]^+$.

Synthesis of 3. Compound **3** was prepared following a procedure similar to that used for compound **2**. The quantities involved and characterization data were as follows: 2,4-dimethylpyrrole (140 mg, 1.47 mmol), 3-dimesitylborylbenzaldehyde (200 mg 0.56 mmol), $BF_3{\cdot}Et_2O$ (13 μL, 0.11 mmol), DDQ (140 mg, 0.62 mmol), triethylamine (0.80 mL, 5.64 mmol), $BF_3{\cdot}Et_2O$ (0.75 mL, 5.64 mmol). Yield: 57 mg, 18%, red solid. ^{1}H NMR (399.99 MHz, $CDCl_3$): δ 7.71 [d, J = 7.6 Hz, 1H (*o*-Ph)], 7.46 [m, 2H (*m*,*o*-Ph)], 7.44 [d, J = 10.2 Hz, 1H (*p*-Ph)], 6.85 [s, 4H (Mes-C-H)], 6.01 [s, 2H (α-pyrrolic H)], 2.54 [s, 6H (β-CH_3)], 2.37, 2.07 [s, 18H (Mes-CH_3)], 1.45 (s, 6H, α-CH_3). ^{13}C NMR (100.00 MHz, $CDCl_3$): δ 155.9, 147.2, 143.3, 142.3, 141.7, 140.8, 139.4, 137.5, 135.9, 135.3, 132.1, 131.9, 129.2, 128.8, 121.7, 30.1, 23.9, 21.6, 15.5. ^{11}B NMR (160 MHz, $CDCl_3$): δ 69.8 (bs), 0. 99 (t, J = 36, 36 Hz). ^{19}F NMR (376 MHz, $CDCl_3$): δ −146.3 (m). HRMS (Q-TOF): calcd ($C_{37}H_{40}B_2F_2N_2Na$), 595.3243 Da; found, 595.3243 Da $[M + Na]^+$.

■ ASSOCIATED CONTENT

Ⓢ Supporting Information

Additional text, figures, tables, and CIF files giving crystal structures, experimental procedures, characterization data, and DFT computational data. This material is available free of charge via the Internet at http://pubs.acs.org.

■ AUTHOR INFORMATION

Corresponding Author

*E-mail: thilagar@ipc.iisc.ernet.in.

Notes

The authors declare no competing financial interest.

■ ACKNOWLEDGMENTS

P.T. thanks CSIR and DST for financial support. C.A.S.P. thanks IISc for SRF, and S.M. thanks CSIR for a Shyama Prasad Mukherjee Fellowship.

■ REFERENCES

(1) (a) Yamaguchi, S.; Wakamiya, A. *Pure Appl. Chem.* **2006**, *78*, 1413. (b) Hudson, Z. M.; Wang, S. *Acc. Chem. Res.* **2009**, *42*, 1584. (c) Jäkle, F. *Chem. Rev.* **2010**, *110*, 3985. (d) Hudson, Z. M.; Wang, S. *Dalton Trans.* **2011**, *40*, 7805. (e) Li, D.; Zhang, H.; Wang, Y. *Chem. Soc. Rev.* **2013**, *42*, 8416. (f) Reus, C.; Weidlich, S.; Bolte, M.; Lerner, H.-W.; Wagner, M. *J. Am. Chem. Soc.* **2013**, *135*, 12892.

(2) (a) Entwistle, C. D.; Marder, T. B. *Chem. Mater.* **2004**, *16*, 4574. (b) Wang, Z. B.; Helander, M. G.; Qiu, J.; Puzzo, D. P.; Greiner, M. T.; Hudson, Z. M.; Wang, S.; Liu, Z. W.; Lu, Z. H. *Nat. Photonics* **2011**, *5*, 753.

(3) Yamaguchi, S.; Akiyama, S.; Tamao, K. *J. Am. Chem. Soc.* **2001**, *123*, 11372.

(4) (a) Hudnall, T. W.; Chiu, C.-W.; Gabbai, F. P. *Acc. Chem. Res.* **2009**, *42*, 388. (b) Zhao, H.; Leamer, L. A.; Gabbai, F. P. *Dalton Trans.* **2013**, *42*, 8164.

(5) (a) Liu, Z.-Q.; Shi, M.; Li, F.-Y.; Fang, Q.; Chen, Z.-H.; Yi, T.; Huang, C.-H. *Org. Lett.* **2005**, *7*, 5481. (b) Sundararaman, A.; Victor, M.; Varughese, R.; Jäkle, F. *J. Am. Chem. Soc.* **2005**, *127*, 13748. (c) You, Y.; Park, S. Y. *Adv. Mater.* **2008**, *20*, 3820. (d) Zhao, Q.; Li, F.; Liu, S.; Yu, M.; Liu, Z.; Yi, T.; Huang, C. *Inorg. Chem.* **2008**, *47*, 9256. (e) Xu, W.-J.; Liu, S.-J.; Zhao, X.-Y.; Sun, S.; Cheng, S.; Ma, T.-C.; Sun, H.-B.; Zhao, Q.; Huang, W. *Chem.—Eur. J.* **2010**, *16*, 7125. (f) Wade, C. R.; Broomsgrove, A. E. J.; Aldridge, S.; Gabbai, F. P. *Chem. Rev.* **2010**, *110*, 3958. (g) Schmidt, H. C.; Reuter, L. G.; Hamacek, J.; Wenger, O. S. *J. Org. Chem.* **2011**, *76*, 9081. (h) Xu, W.; Liu, S.-J.; Sun, H.; Zhao, X.; Zhao, Q.; Sun, S.; Cheng, S.; Ma, T.; Zhou, L.; Huang, W. *J. Mater. Chem.* **2011**, *21*, 7572. (i) Song, K. C.; Kim, H.; Lee, K. M.; Lee, Y. S.; Do, Y.; Lee, M. H. *Sens. Actuators, B* **2013**, *176*, 850. (j) Xu, W.-J.; Liu, S.-J.; Zhao, X.; Zhao, N.; Liu, Z.-Q.; Xu, H.; Liang, H.; Zhao, Q.; Yu, X.-Q.; Huang, W. *Chem.—Eur. J.* **2013**, *19*, 621.

(6) (a) Maeda, H.; Mihashi, Y.; Haketa, Y. *Org. Lett.* **2008**, *10*, 3179. (b) Pfister, A.; Zhang, G.; Zareno, J.; Horwitz, A. F.; Fraser, C. L. *ACS Nano* **2008**, *2*, 1252. (c) Zhang, G.; Lu, J.; Sabat, M.; Fraser, C. L. *J. Am. Chem. Soc.* **2010**, *132*, 2160. (d) Yang, Y.; Hughes, R. P.; Aprahamian, I. *J. Am. Chem. Soc.* **2012**, *134*, 15221. (e) Kubota, Y.; Tanaka, S.; Funabiki, K.; Matsui, M. *Org. Lett.* **2012**, *14*, 4682. (f) Kalita, H.; Lee, W.-Z.; Ravikanth, M. *J. Org. Chem.* **2013**, *78*, 6285.

(7) (a) Loudet, A.; Burgess, K. *Chem. Rev.* **2007**, *107*, 4891. (b) Ulrich, G.; Harriman, A.; Ziessel, R. *Angew. Chem., Int. Ed.* **2008**, *47*, 1202. (c) Kostereli, Z.; Ozdemir, T.; Buyukcakir, O.; Akkaya, E. U. *Org. Lett.* **2012**, *14*, 3636.

(8) Ziessel, R.; Harriman, A. *Chem. Commun.* **2011**, *47*, 611.

(9) Boens, N.; Leen, V.; Dehaen, W. *Chem. Soc. Rev.* **2012**, *41*, 1130.

(10) Bura, T.; Leclerc, N.; Fall, S.; Léveque, P.; Heiser, T.; Retailleau, P.; Rihn, S.; Mirloup, A.; Ziessel, R. *J. Am. Chem. Soc.* **2012**, *134*, 17404.

(11) Huh, J. O.; Do, Y.; Lee, M. H. *Organometallics* **2008**, *27*, 1022.

(12) (a) Fu, G.-L.; Pan, H.; Zhao, Y.-H.; Zhao, C.-H. *Org. Biomol. Chem.* **2011**, *9*, 8141. (b) Sun, H.; Dong, X.; Liu, S.; Zhao, Q.; Mou, X.; Yang, H. Y.; Huang, W. *J. Phys. Chem. C* **2011**, *115*, 19947. (c) Yin, Z.; Tam, A. Y.-Y.; Wong, K. M.-C.; Tao, C.-H.; Li, B.; Poon, C.-T.; Wu, L.; Yam, V. W.-W. *Dalton Trans.* **2012**, *41*, 11340. (d) Lu, J.; Ko, S.-B.; Walters, N. R.; Wang, S. *Org. Lett.* **2012**, *14*, 5660.

(13) (a) Swamy P, C. A.; Mukherjee, S.; Thilagar, P. *Chem. Commun.* **2013**, *49*, 993. (b) Sarkar, S. K.; Thilagar, P. *Chem. Commun.* **2013**, *49*, 8558.

(14) (a) Xie, X.; Yuan, Y.; Kruger, R.; Broring, M. *Magn. Reson. Chem.* **2009**, *47*, 1024. (b) Swamy P, C. A.; Mukherjee, S.; Thilagar, P. *J. Mater. Chem. C* **2013**, *1*, 4691. (c) Ahrens, J.; Boker, B.; Brandhorst, K.; Funk, M.; Broring, M. *Chem.—Eur. J.* **2013**, *19*, 11382. (d) Swamy P, C. A.; Thilagar, P. *Inorg. Chim. Acta* **2014**, *411*, 97.

(15) Achyuthan, K. E.; Bergstedt, T. S.; Chen, L.; Jones, R. M.; Kumaraswamy, S.; Kushon, S. A.; Ley, K. D.; Lu, L.; McBranch, D.; Mukundan, H.; Rininsland, F.; Shi, X.; Xia, W.; Whitten, D. G. *J. Mater. Chem.* **2005**, *15*, 2648.

(16) (a) Zhang, X.; Xiao, Y.; Qian, X. *Angew. Chem., Int. Ed.* **2008**, *47*, 8025. (b) Long, L.; Lin, W.; Chen, B.; Gao, W.; Yuan, L. *Chem. Commun.* **2011**, *47*, 893. (c) He, H.; Ng, D. K. P. *Org. Biomol. Chem.* **2011**, *9*, 2610. (d) Cao, X.; Lin, W.; Yu, Q.; Wang, J. *Org. Lett.* **2011**, *13*, 6098.

(17) (a) Peng, L.; Wang, M.; Zhang, G.; Zhang, D.; Zhu, D. *Org. Lett.* **2009**, *11*, 1943. (b) Huang, X.; Gu, X.; Zhang, G.; Zhang, D. *Chem. Commun.* **2012**, *48*, 12195.

(18) (a) *SAINT-NT*, version 6.04; Bruker AXS: Madison, WI, 2001. (b) *SHELXTL-NT*, version 6.10; Bruker AXS: Madison, WI, 2000.

(19) Frisch, M. J.; Trucks, G. W.; Schlegel, H. B.; Scuseria, G. E.; Robb, M. A.; Cheeseman, J. R.; Scalmani, G.; Barone, V.; Mennucci, B.; Petersson, G. A.; Nakatsuji, H.; Caricato, M.; Li, X.; Hratchian, H. P.; Izmaylov, A. F.; Bloino, J.; Zheng, G.; Sonnenberg, J. L.; Hada, M.; Ehara, M.; Toyota, K.; Fukuda, R.; Hasegawa, J.; Ishida, M.; Nakajima, T.; Honda, Y.; Kitao, O.; Nakai, H.; Vreven, T.; Montgomery, J. A., Jr.; Peralta, J. E.; Ogliaro, F.; Bearpark, M.; Heyd, J. J.; Brothers, E.; Kudin, K. N.; Staroverov, V. N.; Kobayashi, R.; Normand, J.; Raghavachari, K.; Rendell, A.; Burant, J. C.; Iyengar, S. S.; Tomasi, J.; Cossi, M.; Rega, N.; Millam, N. J.; Klene, M.; Knox, J. E.; Cross, J. B.; Bakken, V.; Adamo, C.; Jaramillo, J.; Gomperts, R.; Stratmann, R. E.; Yazyev, O.; Austin, A. J.; Cammi, R.; Pomelli, C.; Ochterski, J. W.; Martin, R. L.; Morokuma, K.; Zakrzewski, V. G.; Voth, G. A.; Salvador, P.; Dannenberg, J. J.; Dapprich, S.; Daniels, A. D.; Farkas, O.; Foresman, J. B.; Ortiz, J. V.; Cioslowski, J.; Fox, D. J. *Gaussian 09*, revision C.01; Gaussian, Inc.: Wallingford, CT, 2010.

dx.doi.org/10.1021/ic402470a | *Inorg. Chem.* 2014, 53, 4813−4823